ARTICLE

Check for updates

Journal of
Sensor Science and Technology

The Korean Sensors Society

Enhanced Short-Wavelength Infrared Photodetector Based on PbS Quantum Dots with NiO Hole-Extraction Layer

Jinbeom Kwon[1], Suji Choi[2], Donggeon Jung[3], and Daewoong Jung[4,+]

[1]*Department of Semiconductor Engineering, Kyungwoon University, 730, Gangdong-ro, Sandong-eup, Gumi-si, Gyeongsangbuk-do 39160, Republic of Korea*
[2]*School of Electronic and Electrical Engineering, Kyungpook National University, Daegu 41566, Republic of Korea*
[3]*Advanced Mobility System Group, Korea Institute of Industrial Technology (KITECH), Daegu 42994, Republic of Korea*
[4]*College of Nanoscience & Nanotechnology, Department of Nanomechatronics Engineering, Pusan National University, 2 Busandaehak-ro, Busan 46241, Republic of Korea*

Cite This: *J. Sens. Sci. Technol. Vol. 34, No. 6 (2025) 676-681*

https://doi.org/10.46670/JSST.2025.34.6.676

ABSTRACT: With the rapid development of automation technologies such as autonomous driving and smart factories, the demand for reliable infrared photodetectors in light detection and ranging (LIDAR) systems has increased. Conventional epitaxial compound-semiconductor detectors are costly and operate in the near-infrared (NIR) region, which poses safety risks to the human eye. To address these issues, we developed a short-wavelength infrared (SWIR) photodetector based on PbS quantum dots (QDs) that can absorb light in the eye-safe region (1400–1500 nm) through particle size control and low-cost solution processing. However, solvent interference between the QDs and hole-extraction layers reduces film uniformity and stability. In this study, a NiO thin film was deposited by radiofrequency (RF) sputtering as a hole-extraction layer to form a quantum well structure, which improved hole extraction efficiency and infrared transmittance. A ZnO nanoparticle electron-extraction layer was additionally applied to balance charge transport and suppress recombination. The optimized NiO/ZnO dual-layer device exhibited excellent band alignment, enhanced optical transparency, and a high responsivity of 115%. These results demonstrate the feasibility of non-cooled, eye-safe SWIR photodetectors for future autonomous and industrial sensing applications.

KEYWORDS: *PbS QDs, Nickel oxide, SWIR, Photodetector*

1. INTRODUCTION

In recent years, the rapid advancement of automation technologies such as autonomous vehicles, intelligent robotics, and smart factories has led to a growing demand for reliable and high-performance optical sensing systems. Among these, light detection and ranging (LIDAR) sensors have become one of the most essential components, providing accurate three-dimensional mapping and environmental recognition for real-time navigation and safety control [1-3]. The key element that determines the performance of a LIDAR system is the infrared photodetector, which converts incoming optical signals into electrical responses with high sensitivity and a fast response speed. Conventional infrared photodetectors are mainly based on epitaxially grown compound semiconductors such as indium gallium arsenide (InGaAs) [4,5]. Although these materials exhibit excellent electrical and optical properties, their fabrication requires high-vacuum epitaxial processes and lattice-matched substrates, resulting in high production costs and limited scalability [6,7]. Moreover, most InGaAs-based detectors operate in the near-infrared (NIR) wavelength range (900–1100 nm), which can be harmful to the human retina [8,9]. This restricts their practical use in applications such as automotive and industrial automation, where humans are frequently exposed to the operating environment. In overcoming these limitations, short-wavelength infrared (SWIR) photodetectors based on lead-sulfide (PbS) quantum dots (QDs) have attracted significant attention [8-11]. PbS QDs possess a tunable bandgap that

[+]Corresponding author: dwjung@pusan.ac.kr
Received : Oct. 27, 2025, Revised : Nov. 3, 2025, Accepted : Nov. 7, 2025

allows selective absorption in the eye-safe region (1400–1600 nm) through simple control of particle size. Furthermore, PbS QDs can be processed via solution-based fabrication, which enables cost-effective, large-area, and flexible device manufacturing. However, photodetectors fabricated solely by solution processes often suffer from low chemical stability, poor film uniformity, and limited patternability, primarily because of solvent interdiffusion between the QDs and adjacent charge-extraction layers [12-14]. In this study, we propose a PbS QDs-based SWIR photodetector with an optimized charge-extraction structure to address these issues. A nickel oxide (NiO) thin film was deposited by radiofrequency (RF) sputtering as the hole-extraction layer (HEL) to form a quantum-well structure, which facilitates efficient hole extraction and improves optical transmittance in the SWIR region [15-18]. The dense and uniform NiO film formed by sputtering also prevents solvent-induced degradation, ensuring enhanced structural and chemical stability of the QDs layer. Additionally, a zinc oxide (ZnO) nanoparticle electron-extraction layer (EEL) was introduced to create a symmetric carrier transport path, which effectively suppresses charge recombination and improves the overall device responsivity [19]. By optimizing the thickness and annealing conditions of the NiO and ZnO extraction layers, the fabricated photodetector achieved superior band alignment, high infrared transparency, and a maximum responsivity of 115% [8,10,16]. These results confirm that the proposed structure successfully enhances both the optical and electrical performance of the PbS QDs-based SWIR photodetectors [23-25].

2. EXPERIMENTAL

2.1 Synthesis of PbS Quantum Dots

The PbS QDs were synthesized using a modified colloidal hot-injection method, following previously reported procedures with slight adjustments [5-7]. Typically, two precursor solutions were prepared separately: a lead precursor by dispersing 2.4 mmol of PbO in 0.265 mL of oleic acid (OA) and a sulfur precursor by dissolving 0.42 mmol of sulfur powder in OA. Both mixtures were stirred for 30 min at room temperature under an argon (Ar) atmosphere to ensure complete homogenization. Subsequently, the PbO–OA mixture was gradually heated to 200°C and maintained for 1 h to form lead–oleate complexes, followed by vacuum degassing at 100°C for 15 min to remove residual moisture and oxygen [7,18]. After degassing, the S–OA precursor solution, along with 265 μL of trioctylphosphine (TOP), was swiftly injected into the Pb precursor solution under continuous Ar flow. The reaction temperature was held at 120°C for 1 h to promote controlled nucleation and growth of PbS QDs. The resulting black colloidal solution was cooled to room temperature and purified by adding a toluene–ethanol (1:1) mixture, followed by centrifugation at 3000 rpm for 10 min to precipitate the QDs. The supernatant was discarded to remove unreacted species, and the purified PbS QDs were finally redispersed in toluene at a concentration of 20 mg/mL^{-1} for subsequent device fabrication.

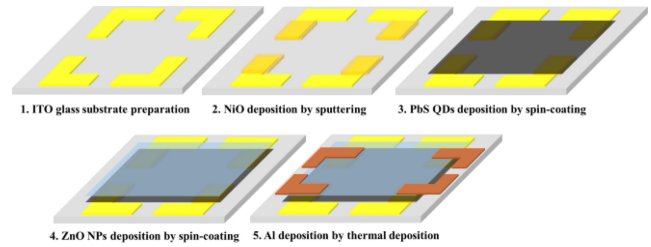

Fig. 1. PbS QD SWIR photodetector with NiO layer.

2.2 Fabrication of PbS Quantum Dots–Based SWIR Photodetector

A transparent glass substrate coated with indium tin oxide (ITO) was used as the anode (Fig. 1). The substrate was sequentially cleaned in acetone, methanol, and deionized (DI) water for 10 min using an ultrasonic cleaner and then dried with nitrogen gas. An HEL was formed by depositing a NiO thin film via RF sputtering. Sputtering was conducted under 200 W power, at an Ar flow rate of 15 sccm, and a chamber pressure of 20 mTorr for 4000 s. After deposition, the film was annealed at 200°C for 3 h to improve its crystallinity and reduce defects [15-18]. A photoactive layer of PbS QDs was deposited by a solution process using spin coating at 1500 rpm for 30 s, followed by annealing at 95°C for 30 min [9-11]. Next, an EEL was fabricated by spin-coating a solution of ZnO nanoparticles (NPs) at 3000 rpm for 60 s, followed by annealing at 80°C for 30 min [19]. Finally, the Al cathode was deposited through a shadow mask using a thermal evaporator, which completed the fabrication of the photodetector having a device structure of ITO/NiO/PbS QDs/ZnO NPs/Al. The active area of the device was defined as the overlapping region between the ITO anode and the Al cathode, covering approximately 3 × 3 mm^2. For reference and comparison, additional devices were fabricated without the NiO layer and annealing to investigate the effects of HEL and thermal annealing on device performance.

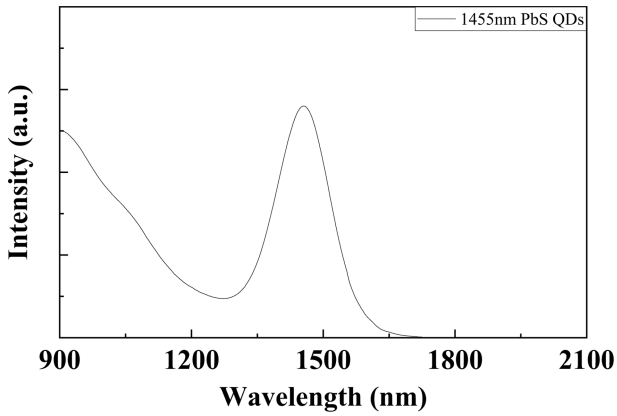

Fig. 2. Absorbance analysis of synthesized PbS QDs.

3. RESULTS AND DISCUSSIONS

3.1 Characteristics of synthesized PbS QDs

Optical characteristics of the synthesized PbS QDs were analyzed using ultraviolet-visible-near infrared (UV–Vis–NIR) absorbance spectroscopy. In Fig. 2, PbS QDs exhibit a distinct absorption peak centered at 1455 nm with a full width at half maximum (FWHM) of 107 nm [5-7]. This relatively narrow bandwidth indicates uniform size distribution of the QDs and confirms their ability to selectively absorb light in the SWIR region near 1.5 μm, which lies within the eye-safe wavelength range suitable for optical communication and LIDAR sensing applications [2,25].

3.2 Structural and Optical Properties of NiO Thin Films

Structural and optical properties of the deposited NiO thin films were investigated using X-ray diffraction (XRD) and NIR transmittance spectroscopy. For analysis, NiO films were deposited on quartz glass substrates and divided into two groups: as-deposited and annealed at 200°C for 3 h, to examine the annealing effect on transmittance improvement [15-18]. The XRD analysis revealed that the film annealed at 200°C exhibits stronger diffraction peaks, indicating an enhancement in crystallinity compared to that of the as-deposited sample (Fig. 3). The grain size variation of the NiO thin films before and after annealing was evaluated using the Scherrer equation based on XRD analysis [9]:

$$D_{hkl}\ (\mathrm{nm}) = (K \times \lambda) / (\beta \cos \theta). \quad (1)$$

In this equation, K denotes the Scherrer constant; λ is the wavelength of the incident X-ray; β is the FWHM of the selected diffraction peak (in radians); and θ is the Bragg

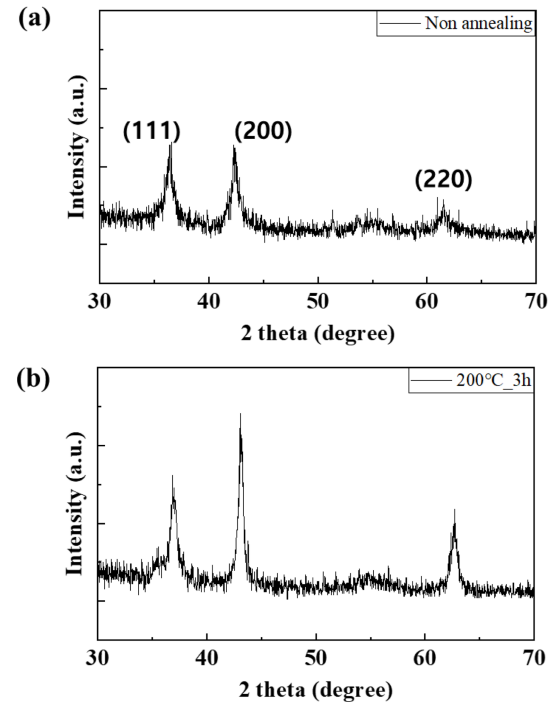

Fig. 3. XRD analysis of the deposited NiO layer (a) non- annealing, and (b) at 200°C for 3 h

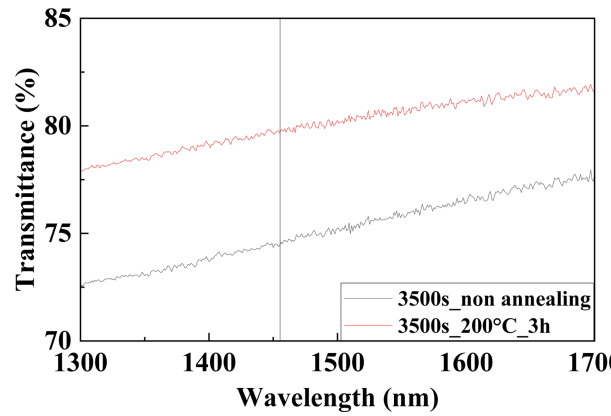

Fig. 4. Transmittance of the deposited NiO layer (a) non-annealing, and (b) 200°C, 3 h

diffraction angle. To analyze the influence of thermal treatment on crystallite growth, the (200) diffraction peak located at $2\theta = 43.3°$ was selected. Using K = 0.94 and λ = 0.15418 nm (Cu Kα radiation), the FWHM values were 0.73° for the as-deposited film and 0.60° for the annealed sample. From these results, the corresponding average crystallite sizes were calculated as approximately 12.2 nm and 15.9 nm, respectively. The increase in grain size after annealing suggests improved crystallinity and reduced lattice imperfections within the NiO film[16-18]. The optical transmittance spectra (Fig. 4) further demonstrate that the annealed NiO film exhibits approximately 5.1% higher transmittance in the 1455 nm wavelength region,

which corresponds to the absorption wavelength of PbS QDS. This enhancement is likely due to the increase in grain size and consequent reduction in grain boundaries, which mitigate light scattering within the film, thereby improving infrared transparency.

3.3 Characteristics of fabricated SWIR photodetector

Electrical and photoresponse characteristics of the fabricated PbS QDs–based SWIR photodetectors were evaluated in an optical test chamber. Each device was mounted on a probe station, and current–voltage (I–V) measurements were performed using a source meter unit (SMU, B2902A, Keysight) under an applied bias of 3 V. An infrared light source (Thorlabs, SLS202L/M) was used to compare the current variations under illuminated and dark conditions to assess the photoresponse behavior of each device. To investigate the effect of the NiO HEL and thermal annealing process on device performance, three types of photodetectors were fabricated under identical conditions: a device without NiO, a device with non-annealed NiO, and a device with a NiO layer annealed at 200°C for 3 h. As shown in Fig. 5(c), the device incorporating the annealed NiO layer exhibited the highest photocurrent, measuring a light current of approximately 1.29 μA and a dark current of 0.6 μA. The non-annealed NiO device showed a moderate response of 0.85 μA, whereas the NiO-free device had the lowest photocurrent of around 0.58 μA [8-10]. This improvement is primarily attributed to the enhanced crystallinity and reduced structural defects in the NiO layer after thermal annealing, which facilitate efficient hole extraction and charge transport across the interface. In addition, the annealed NiO film exhibited higher optical transmittance, allowing a greater amount of infrared light to reach the PbS QDs layer. This improved transparency is a result of grain growth and reduction of grain boundaries, which suppress optical scattering and enhance infrared transmission in the SWIR range (~1455 nm). Consequently, a larger number of photons are absorbed by the PbS QDs, leading to an increase in the generation of electron–hole pairs. Annealing also promotes structural homogenization and stabilizes the surface energy levels of the NiO layer, thereby lowering the potential barrier to hole transport at the PbS QDs/NiO interface. This yields a smoother, lower-resistance pathway for hole extraction, minimizing charge trapping and loss during carrier transport toward the ITO electrode. Moreover, the combination of the NiO HEL and ZnO nanoparticles (ZnO NPs) EEL effectively enhance charge separation within the active layer. ZnO serves as an n-type pathway for electrons, whereas NiO acts as a p-type pathway for holes, and together, they reduce the probability of electron–

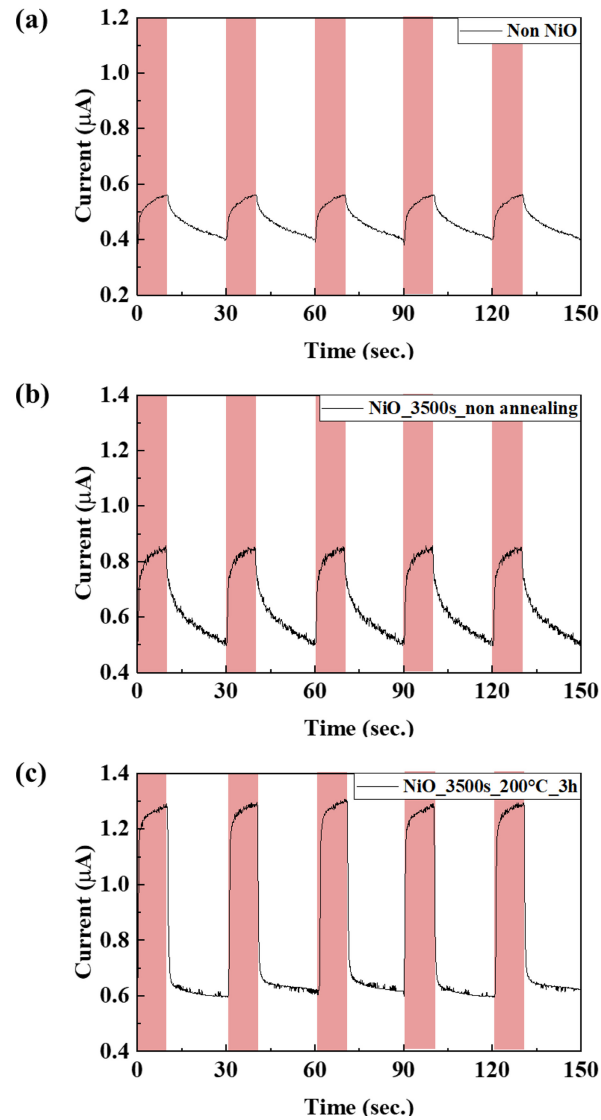

Fig. 5. Photoresponse characteristics of PbS QD-based photodetectors with different NiO conditions.

hole recombination. The annealed NiO film, having fewer defect states, further suppresses interface trapping, enabling the rapid separation and extraction of electrons and holes from their respective electrodes. This synergistic interaction between the NiO and ZnO layers improves charge-transport efficiency and temporal response. Overall, the annealing treatment of the NiO layer simultaneously provides 1) improved infrared transmittance, 2) enhanced hole extraction efficiency, and 3) effective charge separation in cooperation with the ZnO NPs, leading to substantial improvements in photocurrent, sensitivity, response speed, and device stability.

$$\text{Photoresponse (\%)} = \frac{I_{light} - I_{dark}}{I_{dark}} \times 100 \quad (2)$$

As shown in Fig. 6, the photodetector with annealed NiO

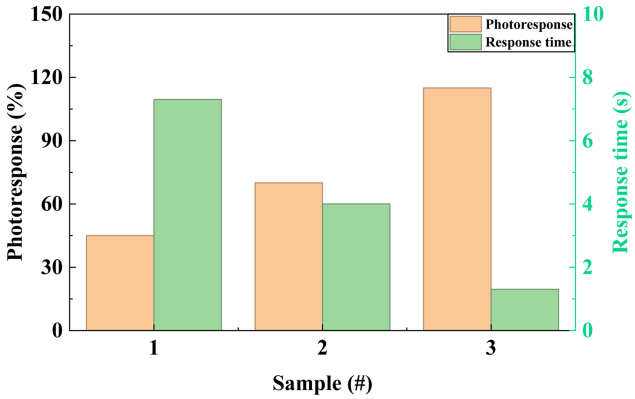

Fig. 6. Photoresponse and response time characteristics of the fabricated SWIR photodetectors.

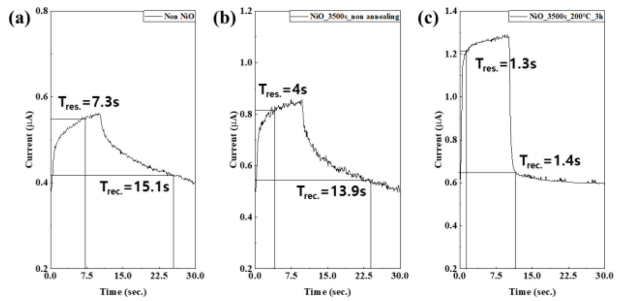

Fig. 7. Real-time response and recovery curve of the sensor, indicating T_{90} response and recovery times. (a) non-NiO, (b) NiO-non annealing, and (c) NiO-annealing.

Table 1. Performance comparison of SWIR sensors fabricated in this study

Parameter	Non NiO	NiO (Non annealing)	NiO (Annealing)
Current variance (μA)	0.16	0.35	0.66
Maximum response (%)	40	75	115
Response time (s)	7.3	4	1.3
Recovery time (s)	15.1	13.9	1.4

exhibits a photoresponse of ~115%, approximately 1.64 times higher than that of the non-annealed NiO device (75%) and 2.87 higher than that of the non-NiO device (40%) [16,17]. As shown in Fig. 7, the annealed NiO device has the fastest rise and decay times of 1.3 s and 1.4 s, respectively, whereas the other devices exhibit slower and noisier responses due to inefficient carrier extraction and enhanced interfacial recombination [15-18]. These results clearly demonstrate that a thermally optimized NiO layer enhances both the optical transparency and hole-transport capability of the device and when combined with ZnO NPs, effectively suppresses charge recombination, leading to improved sensitivity, faster response, and superior overall stability of the SWIR photodetector.

4. CONCLUSIONS

In this study, PbS QDs-based SWIR photodetectors incorporating a NiO HEL and a ZnO NPs EEL were successfully fabricated and characterized. The optical analysis of the synthesized PbS QDs revealed a distinct absorption peak at 1455 nm with a narrow FWHM of 107 nm, confirming their potential for eye-safe infrared detection in the 1.45 μm range. Structural and optical analyses of the NiO thin films demonstrated that thermal annealing at 200°C for 3 h effectively increased the grain size from 12.2 nm to 15.9 nm, leading to enhanced crystallinity and reduced grain boundary density. As a result, the infrared transmittance at 1455 nm improved by approximately 5.1%, primarily because of grain growth and suppression of light scattering at the grain boundaries. These improvements enabled a greater amount of infrared light to reach the PbS QDs layer, thereby increasing photon absorption and carrier generation. Electrical and photoresponse measurements confirmed that the annealed NiO device exhibited the highest performance, with a photocurrent of 1.29 μA and a photoresponse of 115%, which is approximately 1.6 times higher than that of the non-annealed NiO device and nearly three times higher than that of the NiO-free device. Additionally, the annealed NiO photodetector showed faster rise and decay times (1.3 s and 1.4 s), attributed to reduced interfacial traps and more efficient charge extraction. These results clearly demonstrate that annealing-induced improvements in NiO crystallinity and transmittance significantly enhance both hole transport and charge separation efficiency. The NiO and ZnO NPs, combined, effectively suppress electron–hole recombination, resulting in improved sensitivity, faster response, and greater device stability. Overall, the findings of this study suggest that thermally optimized NiO thin films serve as an effective HEL for solution-processed PbS QDs SWIR photodetectors, offering a promising route for the development of low-cost, eye-safe, and high-performance infrared sensing devices applicable to LIDAR and industrial automation systems.

CRediT Authorship Contribution Statement

Jinbeom Kwon: Conceptualization, Methodology, Investigation, Data Curation, Writing – Original Draft. **Suji Choi:** Investigation, Formal Analysis, Validation, Visualization. **Donggeon Jung:** Methodology, Writing, Review & Editing. **Daewoong Jung:** Project administration, Supervision.

Declaration of Competing Interest

The authors declare that they have no competing financial interests or personal relationships that may have influenced the work reported in this study.

Acknowledgements

This work was supported by a New Faculty Research Grant of Pusan National University, 2025 and This study has been conducted with the support of the Korea Institute of Industrial Technology (KITECH) as Development of artificial intelligence-based hydrogen sensor to ensure fuel cell vehicle safety in real driving environments (Kitech UR-25-0005).

REFERENCES

[1] S. Gunapala, B. Levine, D. Ritter, R. Hamm, M. Panish, InGaAs/InP long-wavelength quantum well infrared photodetectors, Appl. Phys. Lett. 58 (1991) 2024–2026.
[2] T. Rauch, M. Böberl, S.F. Tedde, J. Fürst, M.V. Kovalenko, G. Hesser, et al., Near-infrared imaging with quantum-dot-sensitized organic photodiodes, Nat. Photon. 3 (2009) 332–336.
[3] Y. Takano, M. Masuda, K. Kobayashi, K. Kuwahara, S. Fuke, S. Shirakata, Epitaxial growth of InGaAs on misoriented GaAs (100) substrate by metal organic vapor phase epitaxy, J. Cryst. Growth 236 (2002) 31–36.
[4] S. Hyder, R. Saxena, S. Chiao, R. Yeats, Vapor-phase epitaxial growth of InGaAs lattice matched to (100) InP for photodiode application, Appl. Phys. Lett. 35 (1979) 787–789.
[5] J.W. Lee, D.Y. Kim, S. Baek, H. Yu, F. So, Inorganic UV–Visible–SWIR broadband photodetector based on monodisperse PbS nanocrystals, Small 12 (2016) 1328–1333.
[6] M.A. Hines, G.D. Scholes, Colloidal PbS nanocrystals with size-tunable near-infrared emission: observation of post-synthesis self-narrowing of the particle size distribution, Adv. Mater. 15 (2003) 1844–1849.
[7] H. Fu, S.-W. Tsang, Y. Zhang, J. Ouyang, J. Lu, K. Yu, et al., Impact of the growth conditions of colloidal PbS nanocrystals on photovoltaic device performance, Chem. Mater. 23 (2011) 1805–1810.
[8] J.-B. Kwon, S.-W. Kim, B.-H. Kang, S.-H. Yeom, W.-H. Lee, D.-H. Kwon, et al., Air-stable and ultrasensitive solution-cast SWIR photodetectors utilizing modified core/shell colloidal quantum dots, Nano Converg. 7 (2020) 28.
[9] J. Kwon, Y. Ha, S. Choi, D.G. Jung, H.K. An, S.H. Kong, et al., Solution-processed NO_2 gas sensor based on poly(3-hexylthiophene)-doped PbS quantum dots operable at room temperature, Sci. Rep. 14 (2024) 20600.
[10] S. McDonald, P. Cyr, L. Levina, E. Sargent, Photoconductivity from PbS-nanocrystal/semiconducting polymer composites for solution-processable, quantum-size-tunable infrared photodetectors, Appl. Phys. Lett. 85 (2004) 2089–2091.
[11] M. Sulaman, S. Yang, T. Song, H. Wang, Y. Wang, B. He, et al., High-performance solution-processed infrared photodiode based on ternary PbS_xSe_{1-x} colloidal quantum dots, RSC Adv. 6 (2016) 87730–87737.
[12] E. Heves, Y. Gurbuz, PbS colloidal quantum dot photodiodes for SWIR detection, Procedia Eng. 47 (2012) 1426–1429.
[13] E. Hechster, D. Amgar, N. Arad-Vosk, T. Binyamin, A. Sa'ar, L. Etgar, et al., Electrical and optical characterization of quantum dots PbS/TiO_2-based heterojunction as a SWIR detector and a proposed design of PbS/TiO_2 PeLED as a SWIR to visible upconversion device, Mater. Res. Express 6 (2019) 066210.
[14] G. Konstantatos, I. Howard, A. Fischer, S. Hoogland, J. Clifford, E. Klem, et al., Ultrasensitive solution-cast quantum dot photodetectors, Nature 442 (2006) 180–183.
[15] S. Oh, D. Straus, T. Zhao, J.-H. Choi, S.-W. Lee, E. Gaulding, et al., Engineering the surface chemistry of lead chalcogenide nanocrystal solids to enhance carrier mobility and lifetime in optoelectronic devices, Chem. Commun 53 (2017) 728–731.
[16] J. Kwon, S. Kim, J. Lee, C. Park, O. Kim, B. Xu, et al., Uncooled short-wave infrared sensor based on PbS quantum dots using ZnO nanoparticles, Nanomaterials 9 (2019) 926.
[17] H. Zhao, M. Chaker, N. Wu, D. Ma, Towards controlled synthesis and better understanding of highly luminescent PbS/CdS core/shell quantum dots, J. Mater. Chem. 21 (2011) 8898–8904.
[18] F. Ren, H. Zhao, F. Vetrone, D. Ma, Microwave-assisted cation exchange toward synthesis of near-infrared-emitting PbS/CdS core/shell quantum dots with improved quantum yields through a uniform growth path, Nanoscale 5 (2013) 7800–7804.
[19] V. Kumar, H. Sharma, S.K. Singh, S. Kumar, A. Vij, Enhanced near-band-edge emission in pulsed-laser-deposited ZnO/c-sapphire nanocrystalline thin films, Appl. Phys. A 125 (2019) 212.
[20] W. Smith, "Selenium", its electrical qualities and the effect of light thereon, J. Soc. Telegraph Eng. 6 (1877) 423–441.
[21] R.S. Shekhawat, Infrared thermography—A review, Int. J. Eng. Trends Technol. 35 (2016) 287–290.
[22] M. Abulmakarim, I. Rufai, A. Musa, Investigation of the properties of cadmium sulphide thin films for solar cell applications, Int. J. Energy Eng. 4 (2014) 61–67.
[23] F.P. García de Arquer, A. Armin, P. Meredith, E.H. Sargent, Solution-processed semiconductors for next-generation photodetectors, Nat. Rev. Mater. 2 (2017) 16100.
[24] T. Bourlai, N. Kalka, A. Ross, B. Cukic, L. Hornak, Cross-spectral face verification in the short-wave infrared (SWIR) band, Proceedings of the 20th Int. Conf. Pattern Recogn., Istanbul, Turkey, 2010, pp.1343–1347.
[25] A. Gassenq, F. Gencarelli, J. Van Campenhout, Y. Shimura, R. Loo, G. Narcy, et al., GeSn/Ge heterostructure short-wave infrared photodetectors on silicon, Opt. Express 20 (2012) 27297–27303.